

Cobalt-Doped SnS₂ with Dual Active Centers of Synergistic Absorption-Catalysis Effect for High-S Loading Li-S Batteries

Xuejie Gao, Xiaofei Yang, Minsi Li, Qian Sun, Jianneng Liang, Jing Luo, Jiwei Wang, Weihan Li, Jianwen Liang, Yulong Liu, Sizhe Wang, Yongfeng Hu, Qunfeng Xiao, Ruying Li, Tsun-Kong Sham,* and Xueliang Sun*

The application of Li-S batteries is hindered by low sulfur utilization and rapid capacity decay originating from slow electrochemical kinetics of polysulfide transformation to Li₂S at the second discharge plateau around 2.1 V and harsh shuttling effects for high-S-loading cathodes. Herein, a cobalt-doped SnS₂ anchored on N-doped carbon nanotube (NCNT@Co-SnS₂) substrate is rationally designed as both a polysulfide shield to mitigate the shuttling effects and an electrocatalyst to improve the interconversion kinetics from polysulfides to Li₂S. As a result, high-S-loading cathodes are demonstrated to achieve good cycling stability with high sulfur utilization. It is shown that Co-doping plays an important role in realizing high initial capacity and good capacity retention for Li-S batteries. The S/NCNT@Co-SnS₂ cell (3 mg cm⁻² sulfur loading) delivers a high initial specific capacity of 1337.1 mA h g⁻¹ (excluding the Co-SnS₂ capacity contribution) and 1004.3 mA h g⁻¹ after 100 cycles at a current density of 1.3 mA cm⁻², while the counterpart cell (S/NCNT@SnS₂) only shows an initial capacity of 1074.7 and 843 mA h g⁻¹ at the 100th cycle. The synergy effect of polysulfide confinement and catalyzed polysulfide conversion provides an effective strategy in improving the electrochemical performance for high-sulfur-loading Li-S batteries.

1. Introduction

To meet the increasing demand for electric vehicles and portable electronic devices for high energy density, environmentally friendly and low-cost lithium-sulfur (Li-S) batteries with a high theoretical energy density of 2600 Wh kg⁻¹ have received great attention and have been widely regarded as one of the most

promising candidates for the next-generation rechargeable batteries.^[1] Nevertheless, the practical application of Li-S batteries is hindered by several critical challenges. The soluble polysulfides (Li₂S_n, 4 ≤ n ≤ 8) shuttling between anode and cathode, namely, shuttle effects, can cause low coulombic efficiency and rapid capacity decay. The low electronic conductivity of the starting active material (S₈) and the discharge product (Li₂S) can not only be detrimental to the rate performance but also limit the sulfur loading and sulfur utilization. To achieve a high areal capacity of 4 mA h cm⁻² as comparable to the state-of-the-art lithium-ion batteries, a high sulfur loading of more than 3 mg cm⁻² is crucial.^[2] However, the sulfur loadings in most previous reported Li-S batteries with high discharge capacities and long cycling lives are usually below 2 mg cm⁻², which fail to meet the requirements for practical energy density.^[3] Furthermore, the electrochemical conversion from polysulfides to


Li₂S at the second discharge plateau can be significantly limited by the sluggish kinetics of the solid-liquid reaction from polysulfides to Li₂S₂ and solid-solid reaction from Li₂S₂ to Li₂S, leading to an early end of discharge and low sulfur utilization. The resulting problem of low specific discharge capacity is even exacerbated in high-sulfur-loading batteries combining with the challenges of poor ionic and electronic conductivities.^[4]

To overcome the aforementioned challenges, most of the efforts have been devoted to designing multi-functional and multi-architecture cathode materials/cathodes to alleviate the shuttle effect and improve the electrochemical kinetics of sulfur species.^[5] Highly conductive carbon materials with tunable porosity and architectures are most widely used as hosts for sulfur to prepare S/C composites. However, the nonpolar carbon materials show weak interactions with the polysulfide species, leading to inevitable discharge attenuation and poor cycling stability. Recently, polar metal compounds such as metal oxides,^[6] metal nitrides,^[7] and metal polysulfides^[1c,8] were demonstrated as effective polysulfide absorbents to further improve the cycling stability of Li-S batteries. These metal compounds are either in situ grown on the carbon hosts or mixed with carbon materials. Among the possible candidates, SnS₂ exhibits a favorable bonding strength with polysulfides, which allows SnS₂ to efficiently anchor and release polysulfides during charge/discharge

X. Gao, Dr. X. Yang, M. Li, Dr. Q. Sun, J. Liang, J. Luo, J. Wang, Dr. W. Li, Dr. J. Liang, Dr. Y. Liu, S. Wang, R. Li, Prof. X. Sun
Department of Mechanical and Materials Engineering
University of Western Ontario
London, Ontario, N6A 5B9, Canada
E-mail: xsun9@uwo.ca

X. Gao, M. Li, J. Wang, Dr. W. Li, Prof. T.-K. Sham
Department of Chemistry
University of Western Ontario
London, Ontario, N6A 5B7, Canada
E-mail: tsham@uwo.ca

Dr. Y. Hu, Dr. Q. Xiao
Canadian Light Source
44 Innovation Boulevard, Saskatoon, Saskatchewan, S7N 2V3, Canada

 The ORCID identification number(s) for the author(s) of this article can be found under <https://doi.org/10.1002/adfm.201806724>.

DOI: 10.1002/adfm.201806724

cycles.^[8a] Qian and co-workers investigated the electrochemical performance of S/C-SnS₂ composites with different mass contents of ultrathin SnS₂. Benefiting from the synergistic effects of physical confinement by porous carbon and chemical interactions with SnS₂, S/C-SnS₂ composite with 10 wt% of ultrathin SnS₂ nanosheets exhibits excellent cycling stability. However, limited by the slow electrochemical kinetics of conversion from polysulfides to Li₂S at the second discharge plateau (≈ 2.1 V), even a low-sulfur-loading cathode ($1\text{--}1.5$ mg cm⁻²) delivered a sulfur utilization of 65%.^[8a] Therefore, further developing SnS₂-based polar polysulfide absorbents with high sulfur loadings and high sulfur utilization is important. Moreover, accelerating the sluggish electrochemical conversion of polysulfides to Li₂S is of utmost importance to improve polysulfide redox kinetics, promise low polarization, and reduce the overall overpotential, and then further improve sulfur utilization as well as increase specific discharge capacity. In any case, cobalt compounds deliver a promising catalyst for Li-S batteries because of the mechanism in which the polar surface accelerates polysulfides redox has been clearly revealed. For example, Qian's group studies the Co-based compounds, exhibiting that CoP has a low overpotential for polysulfide transformation.^[9] In addition, CoP and CoS₂ showed strong interactions with polysulfide and dynamic enhancement in polysulfide redox reactions.^[10] The polysulfide redox reactions including the solid-liquid step and the liquid-solid step are thus facilitated. The voltage polarization during the electrochemical process is also reduced.

This work rationally combines the merits between the polysulfide-confining SnS₂ and the catalytic cobalt compounds by growing cobalt-doped SnS₂ on N-doped carbon nanotubes (hereafter referred to as NCNT@Co-SnS₂) as the host for sulfur cathode (S/NCNT@Co-SnS₂). Alleviated polysulfide shuttling effect, improved cycling stability, and enhanced sulfur utilization are achieved comparing to S/NCNT and undoped S/NCNT@SnS₂ electrodes. The S/NCNT@Co-SnS₂ electrode delivers a high capacity of 1337.1 mA h g⁻¹ and remains 1004.3 mA h g⁻¹ after 100 cycles at a current density of 1.3 mA cm⁻², which is superior to the control electrode of undoped S/NCNT@SnS₂ electrode (with an initial capacity of 1074.7 and 843 mA h g⁻¹ at the 100th cycle). Additionally, the S/NCNT@Co-SnS₂ cathode with a high sulfur loading of 3 mg cm⁻² also shows a low capacity attenuation of 0.16% per cycle over 300 cycles at 3.2 mA cm⁻².

2. Results and Discussion

The detailed synthetic procedure of NCNT@Co-SnS₂ can be seen from schematic as shown in **Figure 1a**. First, N-doped carbon nanotubes on carbon paper (CP) (named as CP@NCNT) were synthesized by a spray pyrolysis chemical vapor deposition (SPCVD) method based on previous reports.^[14] This was followed by a solvothermal reaction by mixing SnCl₄·5 H₂O, CoCl₂·6 H₂O, and thioacetamide (TAA) in ethanol at 80 °C to obtain uniform growth of Co-SnS₂ nanoflakes on the NCNTs (NCNT@Co-SnS₂). Further details of the synthetic procedure can be found in the Experimental Section. The synthesis of counterpart without Co-doping named as NCNT@SnS₂ is shown in Figure S1 (Supporting Information), demonstrating

the same structure after the same preparation of NCNT@Co-SnS₂. As shown in the scanning electron microscopy (SEM) images in Figure S2a,b (Supporting Information), pristine CP@NCNT showed a bamboo-like structure with diameters around 20–50 nm and intermittent joints. The SnS₂ nanoflakes were grown and distributed uniformly on the surface of NCNTs for both high-SnS₂-loading NCNTs (NCNT@SnS₂-H, with adding 1.6×10^{-3} M SnCl₄·5 H₂O) in Figure S2c,d (Supporting Information) and low-SnS₂-loading NCNTs (NCNT@SnS₂, with adding 0.8×10^{-3} M SnCl₄·5 H₂O) in Figure S3a–c (Supporting Information). Transmission electron microscopy (TEM) images of NCNT@SnS₂ indicated the continuous coverage of SnS₂ on top of the NCNT surface (Figure S3d–f, Supporting Information). The average thickness of the SnS₂ layer on NCNT@SnS₂ was ≈ 50 nm. The fringe interval of the SnS₂ was 0.59 nm, consistent with the interplanar spacing of the (001) crystal planes of hexagonal phase SnS₂.^[8a] The corresponding elemental mapping confirmed the uniform distribution of C, Sn, and S at NCNT@SnS₂ (Figure S3g–j, Supporting Information). After Co-doping on NCNT@SnS₂, the morphology and crystalline structure of SnS₂ remained unchanged (Figure 1b–f). However, the corresponding energy dispersive X-ray spectroscopy (EDX) analysis (Figure 1g) and elemental mappings (Figure 1h–l) together with the color change of powder from grey to reddish (Figure S4, Supporting Information) suggested the successful doping of Co element, achieving the designed NCNT@Co-SnS₂ sample. The retention of SnS₂ crystalline structure could be mainly attributed to the similar radii of Co (+2) and Sn (+4). In addition, ex situ X-ray absorption near edge structure (XANES) is an element and chemical specific local probe that tracks the oxidation state and bonding with neighboring atom via the modulation of its absorption coefficients above an absorption edge. XANES spectra of Sn L₃-edge and Co K-edge with total electron yield (TEY) for both NCNT@SnS₂ and NCNT@Co-SnS₂ before sulfur impregnation are shown in Figure S5a (Supporting Information). The similar Sn L₃-edge profiles and peak positions again confirmed the successful loading of SnS₂ on NCNTs and the unchanged local valence structure of SnS₂ with Co-doping. Moreover, according to the reference spectra of Co K-edge of LiCoO₂ and CoS₂, we can deduce that the Co element doped on the NCNT@Co-SnS₂ was in the form of Co²⁺ (Figure S5b, Supporting Information).

The effects of SnS₂ on improving the electrochemical performance was investigated by cycling test at a current density of 1.3 mA cm⁻². As shown in Figure S6a (Supporting Information), the S/NCNT exhibited a typical two-plateau discharge profile in an ether-based electrolyte in the voltage window of 1.7–2.8 V. The plateaus located at around 2.3 and 2.1 V were related to the two-step reduction from S₈ to Li₂S.^[11] The presence of SnS₂ introduced an additional plateau at ≈ 2.2 V for electrodes with low or high SnS₂ loadings (S/NCNT@SnS₂ and S/NCNT@SnS₂-H), attributable to the reduction of SnS₂ to SnS in the designated voltage window. As shown in Figure S6b (Supporting Information), the S/NCNT, S/NCNT@SnS₂-H, and S/NCNT@SnS₂ electrodes delivered an initial discharge capacity of 1078.9, 1016.9, and 1328.7 mA h g⁻¹, respectively. However, excluding the discharge capacity contributed from the reduction of SnS₂ (≈ 50 mA h g⁻¹; Figure S7a, Supporting Information) and LiNO₃ decomposition below ≈ 1.7 V, the

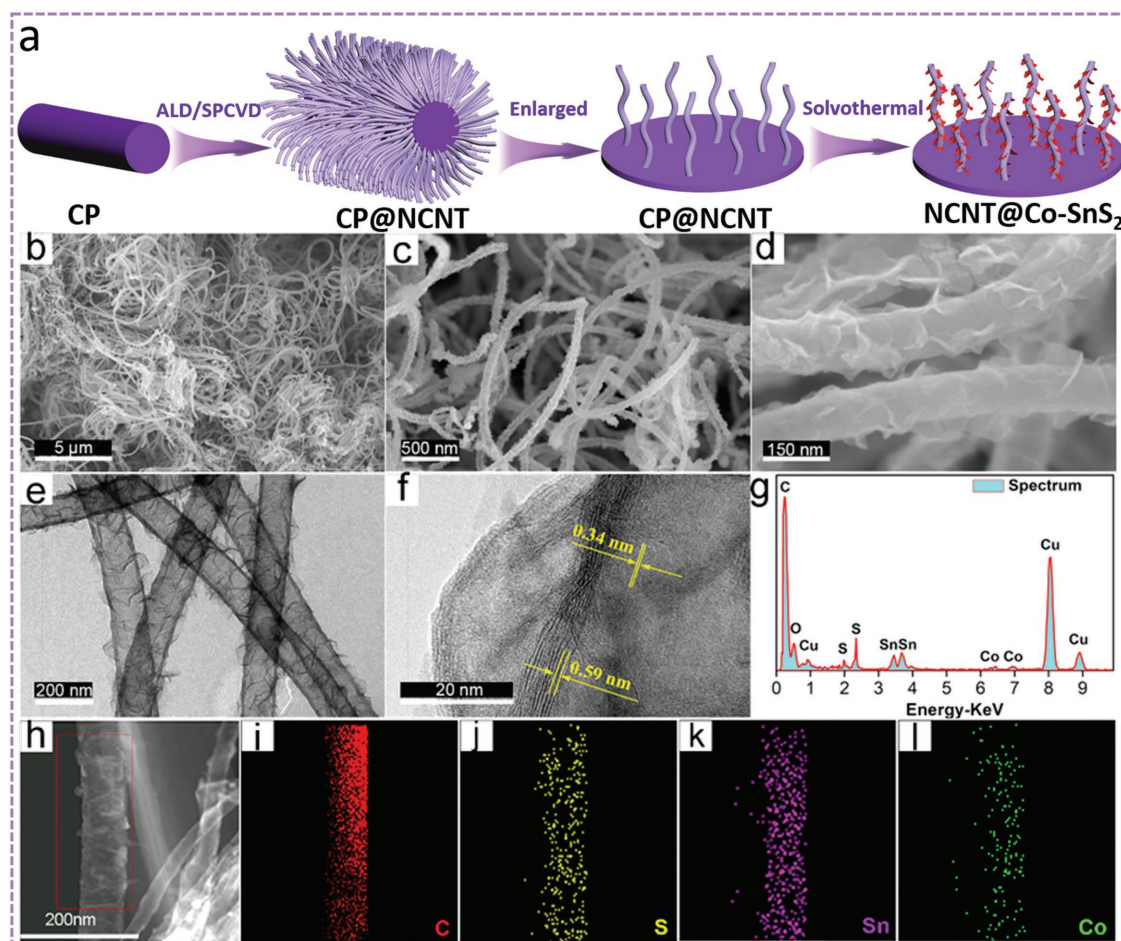


Figure 1. a) Schematic illustrations of the synthesis process of NCNT@Co-SnS₂. Characterizations of NCNT@Co-SnS₂: b–d) SEM images and e, f) TEM images at different magnifications; g) EDX spectrum; and h) TEM image and i–l) corresponding elemental mappings for C, S, Sn, and Co elements.

S/NCNT@SnS₂ and S/NCNT@SnS₂-H electrodes showed a similar discharge capacity (the capacity delivered by reduction of sulfur) around 1070 mA h g⁻¹ in the initial cycle. After stable cycling for 100 cycles, the S/NCNT, S/NCNT@SnS₂-H, and S/NCNT@SnS₂ cells retained a discharge capacity of 630.8, 663.4, and 843.1 mA h g⁻¹, corresponding to a capacity retention of 59%, 62%, and 78%, respectively. The improved cycling performance within SnS₂ loading was mainly attributed to the strong chemical interactions between SnS₂ and polysulfides that reduced the loss of sulfur active material from the shuttling effects.^[8b] Further increasing the concentration of SnS₂ leads to a lower conductivity of the electrode, which limited the electron transport and the transformation reactions between the sulfur, polysulfides, and Li₂S, resulting in a low cycling stability. With this in mind, the low concentration of SnS₂ is chosen as the substrate to investigate the influence of Co-doping.

To further investigate the effects of Co-doping, the electrochemical performance of S/NCNT@SnS₂ and S/NCNT@Co-SnS₂ has been examined and is shown in **Figure 2**. Figure 2a shows the cyclic voltammetry (CV) profiles for the S/NCNT@SnS₂ and S/NCNT@Co-SnS₂ electrodes. Three cathodic peaks and one anodic peak were observed in the selected voltage window, corresponding to the reduction of sulfur to long-order

polysulfides at ≈2.3 V, reduction of SnS₂ to SnS at ≈2.2 V, further reduction of polysulfides to Li₂S₂/Li₂S at ≈2.0 V, and reversible oxidation of Li₂S/Li₂S to sulfur at 2.5 V, respectively.^[11b,12] It should be noted that the peak corresponding to SnS₂ reduction became weaker after Co-doping, which is attributed to the partial substitution of Sn sites by Co in the SnS₂. The S/NCNT@Co-SnS₂ electrode exhibited sharper cathodic and anodic peaks as well as reduced polarization compared with the S/NCNT@SnS₂ electrode, indicating improved electrochemical reaction kinetics by Co-doping. The electrochemical impedance spectroscopy (EIS) analysis gave similar hints. As shown in Figure S8 (Supporting Information), while the two electrodes exhibited similar ohmic resistance (R_s) around 5 Ω, the S/NCNT@Co-SnS₂ electrode showed significantly smaller charge transfer resistance (R_{ct}) of 43.5 Ω than that of the S/NCNT@SnS₂ electrode (58.0 Ω). R_{ct} is closely related to the chemical reaction activation energy, and the 25% reduction can be an evidence for the positive role of Co-doping in enhancing electrochemical kinetics. Consistent with the CV results, cobalt-doped SnS₂ possessed a catalytic effect for the electrochemical transformation reactions among the sulfur species.

The charge/discharge profiles of S/NCNT@Co-SnS₂ and S/NCNT@SnS₂ electrodes at the first cycle are shown in

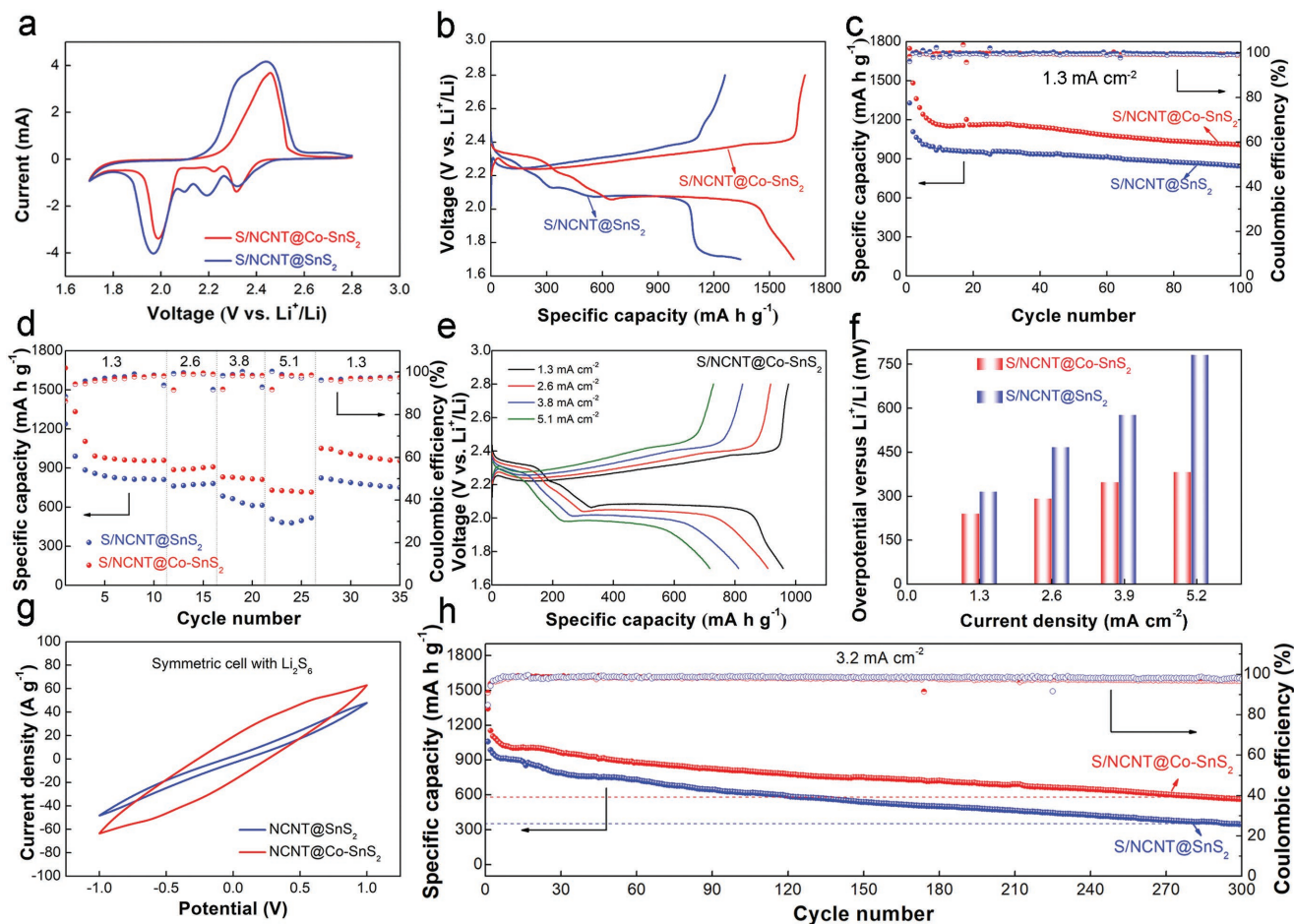


Figure 2. Comparison on the electrochemical performances of the S/NCNT@SnS₂ and S/NCNT@Co-SnS₂ electrodes with an S loading of 3 mg cm⁻²: a) CV profiles (second cycle); b) discharge/charge profiles; c) cycling performance at 1.3 mA cm⁻² and (d) rate performance at various current densities ranging from 1.3 to 5.1 mA cm⁻²; e) corresponding discharge/charge profiles at the different current densities; f) evolution of the overpotential at various current densities from 1.3 to 5.1 mA cm⁻²; g) CV curves of symmetric cells using Li₂S₆ electrolyte; and h) long-term cycling performance at 3.2 mA cm⁻² for 300 cycles.

Figure 2b. Both electrodes showed three discharge plateaus in the selected voltage window, correspondent to the CV results. Notably, the third plateau at 2.03 V of the S/NCNT@Co-SnS₂ electrode was much longer than that of the S/NCNT@SnS₂ electrode, suggesting an improved sulfur utilization during the interconversion from Li₂S₄ to Li₂S. The detail catalytic mechanism will be further clarified in the following discussion. Due to the prolonged discharge plateau at 2.03 V, the S/NCNT@Co-SnS₂ delivered a high initial capacity of about 1337.1 mA h g⁻¹ excluding a capacity of ≈410 mA h g⁻¹ from Co-SnS₂ (Figure S7b, Supporting Information). The much higher capacity than that of the S/NCNT@SnS₂ electrode (1074.7 mA h g⁻¹) indicated an improved sulfur utilization with Co-doping. The improved sulfur utilization is further demonstrated by comparing the SEM images of two electrodes after the first discharge and washed with 1,2-dimethoxymethane (DME) solvent. As shown in Figure S9a,b (Supporting Information), the S/NCNT@SnS₂ electrode was almost covered by a dense film of reaction side products. The discharge reaction would terminate as the surface of SnS₂ has been blocked, thus leading to low sulfur utilization. In contrast, porous

morphology of the S/NCNT@Co-SnS₂ electrode was maintained, with Li₂S₂ and Li₂S selectively deposited along the NCNT@Co-SnS₂ (Figure S9c,d, Supporting Information). The Co-doping was evidently playing an important role in facilitating thorough electrochemical reactions. Moreover, since the discharge products grew along the NCNT@Co-SnS₂ leaving clear Li⁺ channels for Li⁺ transport, it is beneficial for rate performance. Importantly, the S/NCNT@Co-SnS₂ was able to remain catalytically active during repeated charge/discharge process. Even after 20 cycles, the S/NCNT@Co-SnS₂ electrode still maintained a longer discharge plateau for Li₂S conversion at ≈2.03 V (giving overall capacity of 1128.7 mA h g⁻¹ vs 846.7 mA h g⁻¹ for S/NCNT@SnS₂), which was desirable to maintain high discharge capacity output during long-term cycling as shown in Figure S10 (Supporting Information). More importantly, the cycling performance of Li-S batteries assembled with S/NCNT@Co-SnS₂ and S/NCNT@SnS₂ electrode was investigated at a current density of 1.3 mA cm⁻², and the S/NCNT@Co-SnS₂ electrode could still maintain 1004.3 mA h g⁻¹ after 100 cycles, ≈20% higher than that of the S/NCNT@SnS₂ electrode (843 mA h g⁻¹ after 100 cycles)

with a sulfur loading of 3 mg cm^{-2} at 1.3 mA cm^{-2} , as shown in Figure 2c.

The interaction between the hosts and polysulfides was studied by a static adsorption experiment, where the yellowish Li_2S_6 was used to represent the soluble polysulfides. As shown in Figure S11 (Supporting Information), for this test, $5 \times 10^{-3} \text{ M}$ Li_2S_6 solution (1 mL) was used as a reference. Then pure NCNT powder, NCNT@ SnS_2 , and NCNT@Co- SnS_2 were immersed into a Li_2S_6 solution separately for 10 h to monitor the color changes. It is obvious that both NCNT@ SnS_2 and NCNT@Co- SnS_2 decolored the Li_2S_6 solution, while the NCNT showed no obvious effect. Notably, the resulting solution with NCNT@Co- SnS_2 became almost colorless, while trace amount of yellow color was still observed for the solution with NCNT@ SnS_2 . This indicated the enhanced effect on polysulfide adsorption by Co-doping. The outstanding polysulfide trapping capability can be a direct reason for the superior cycling performance of the S/NCNT@Co- SnS_2 electrode. To further understand the reasons for the different cycling stabilities, the S/NCNT@ SnS_2 and S/NCNT@Co- SnS_2 cells were disassembled after cycling for morphological analysis by SEM. As shown in Figure S12 (Supporting Information), similar to the morphology of S/NCNT@ SnS_2 and S/NCNT@Co- SnS_2 electrodes after the first cycle, the discharge products selectively grow along the S/NCNT@Co- SnS_2 electrode (Figure S12e,f, Supporting Information), which maintain Li^+ channels for Li^+ transport. In contrary, the growth of discharge products shows no selectivity on S/NCNT@ SnS_2 electrode as exhibited in Figure S12a,b (Supporting Information), which blocked the Li^+ transport channels, hence restricted Li^+ transport. Moreover, due to the improved chemical interaction between NCNT@Co- SnS_2 and polysulfides, the free diffusion of polysulfides to the anode side is limited, resulting in less reaction with Li anode and fewer side-products deposited on the anode surface. As shown in Figure S12g,h (Supporting Information), the thickness of the side-products deposited on the Li anode coupled with S/NCNT@Co- SnS_2 electrode was $20 \mu\text{m}$, which was much thinner than its counterpart ($60 \mu\text{m}$; Figure S12c,d, Supporting Information). In summary, the selective deposition of discharge products, stronger interaction between NCNT@Co- SnS_2 and polysulfides, as well as fewer side-products formed on the anode side can well explain the reason for the improvements of the cycling stability for S/NCNT@Co- SnS_2 electrode.

The C-rate performance of S/NCNT@ SnS_2 and S/NCNT@Co- SnS_2 electrodes is further shown in Figure 2d. The S/NCNT@Co- SnS_2 electrode delivered average discharge capacities of 1076, 896, 822, and 722 mA h g^{-1} at current densities of 1.3, 2.6, 3.8, and 5.1 mA cm^{-2} , respectively. A high capacity of 1054 mA h g^{-1} was recovered when the current density returned to 1.3 mA cm^{-2} . However, for S/NCNT@ SnS_2 electrode, the corresponding values were only 882, 771, 641, and 496 mA h g^{-1} at current densities of 1.3, 2.6, 3.8, and 5.1 mA cm^{-2} , respectively, and a capacity of 823 mA h g^{-1} recovered to 1.3 mA cm^{-2} . The improved performance of NCNT@Co- SnS_2 was mainly due to the reduced polarization upon increasing current density. As shown in Figure 2e and Figure S13 (Supporting Information), the overpotential of S/NCNT@Co- SnS_2 electrode and S/NCNT@ SnS_2 is determined by the voltage difference based on the median of second

discharge plateau at different current densities, according to the previous report.^[13] The overpotential can reflect the electrochemical kinetics of sulfur species on different substrates. The evolution of the overpotential at various current densities from 1.3 to 5.1 mA cm^{-2} is thereby shown in Figure 2f. It is obvious that the overpotential of S/NCNT@Co- SnS_2 electrode is smaller than that of S/NCNT@ SnS_2 at all current densities. Particularly, when the current density further increased to 5.1 mA cm^{-2} , the overpotential of S/NCNT@Co- SnS_2 electrode is about 382 mV, which is almost half of its counterpart ($\approx 782 \text{ mV}$), suggesting faster electrochemical kinetics of sulfur species on the S/NCNT@Co- SnS_2 electrode. The smaller overpotential induced by Co-doping is mainly attributed to the improved electrochemical kinetics and well-maintained Li^+ transport channels via the selective deposition of discharge products. This plays an important role in meeting the demand of electrochemical reactions at high current densities.

Moreover, the dynamic effect on the redox conversion of polysulfides was examined by CV with symmetrical Li_2S_6 - Li_2S_6 cells. As shown in Figure 2g, it can be clearly seen that the current density of the cell assembled with NCNT@Co- SnS_2 electrode is two times higher than that of NCNT@ SnS_2 electrodes, demonstrating that doping Co not only improves the chemical interaction with polysulfides but also dynamically accelerates the electrochemical reactions of lithium polysulfides.^[10b,14] In addition, the long-term cycling performance of the Li-S batteries assembled with S/NCNT@Co- SnS_2 and S/NCNT@ SnS_2 electrodes is further investigated at a higher current density of 3.2 mA cm^{-2} . As shown in Figure 2h, the S/NCNT@Co- SnS_2 electrodes deliver a high initial capacity of 1342 mA h g^{-1} at 3.2 mA cm^{-2} . And a reversible capacity of $1062.3 \text{ mA h g}^{-1}$ is achieved at the fifth cycle after fast capacity decay in the first few cycles. Even after 300 cycles, still a high capacity of 562 mA h g^{-1} is maintained, corresponding to a low capacity attenuation rate of 0.16% per cycle (calculated based on the fifth cycle), demonstrating the excellent cycling stability. The high sulfur utilization and cycling performance is much better than most previously reported high sulfur loading cathodes.^[15] In contrast, the S/NCNT@ SnS_2 electrodes remaining capacity and capacity retention are only 346 mA h g^{-1} and 32.7% (calculated based on the fifth cycle), respectively.^[16] Figure S14 (Supporting Information) demonstrates that the energy efficiency of S/NCNT@Co- SnS_2 electrodes is higher than that of S/NCNT@ SnS_2 electrodes. These results further highlight the merits of cobalt-doped SnS_2 in improving the sulfur utilization and cycling stability via catalyzing the electrochemical kinetics and improving the chemical interaction between polysulfides and host.

To understand the detailed catalytic mechanism and interactions between the polysulfides and Co- SnS_2 , XANES analyses for samples at different charge/discharge states were conducted. The results for the S K-edge (1s) of S/NCNT@ SnS_2 and S/NCNT@Co- SnS_2 with TEY are shown in Figure 3. Before sulfur impregnation, S K-edge of both NCNT@ SnS_2 and NCNT@Co- SnS_2 showed similar profiles and peak positions to the SnS_2 reference, indicating successful loading of SnS_2 on NCNTs and unchanged valence of SnS_2 by Co-doping. After sulfur impregnation, a new peak at 2471.6 eV appeared on the S K-edge spectra for both S/NCNT@ SnS_2

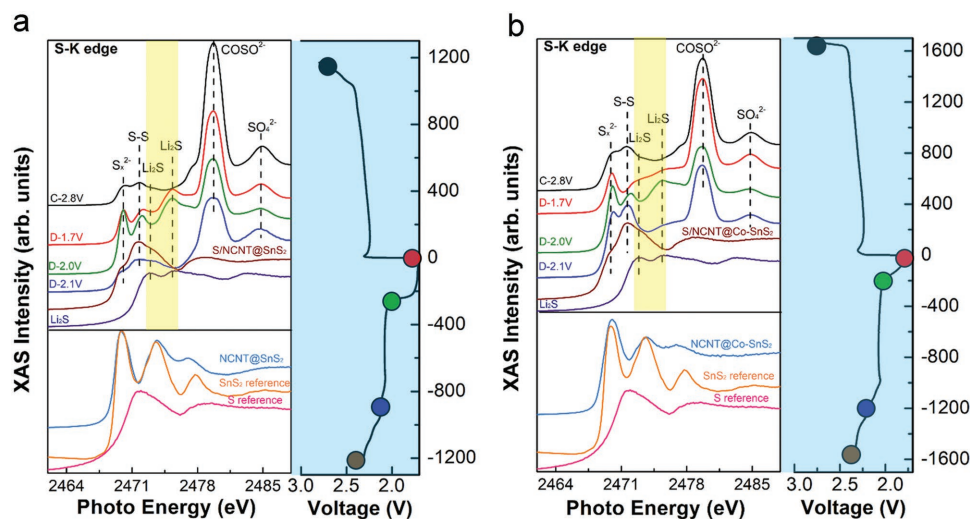


Figure 3. Catalytic mechanisms study on NCNT@Co-SnS₂: S K-edge XANES of a) S/NCNT@SnS₂ and b) S/CP@NCNT@Co-SnS₂ electrodes at different discharge/charge states.

and S/NCNT@Co-SnS₂, attributing to the S 1s to S-S π^* state transition (Figure 3a,b).^[17] At higher discharge state, a pre-edge feature at 2470.0 eV appeared and gradually became stronger, which can be assigned to the S 1s to π^* state transition associated with linear polysulfides.^[17a,18] Subsequently, an emerging peak at 2475.4 eV for Li₂S co-existed with the peaks at 2471.6 and 2471.6 eV, indicating the mixture of Li₂S and polysulfides when discharged to 2.0 V (Figure 3a,b, highlighted by yellow shadings).^[19] Interestingly, the difference between the two electrodes appeared particularly in the voltage range of the second discharge plateau. Without Co-doping (Figure 3a), the polarization for the S/NCNT@SnS₂ electrodes increased instantly at this point and the discharge process terminated in few seconds, leading to a negligible change in S K-edge from 2.0 to 1.7 V. However, the behavior was quite different for S/NCNT@Co-SnS₂ electrode. When discharged from 2.0 to 1.7 V, the feature located at 2471.6 eV for S-S disappeared, while a new feature appeared at 2472.9 eV. This is an indication of the complete conversion of polysulfides to the final discharge product Li₂S (Figure 3b, highlighted by yellow shadings).^[18a,20] This result indicates that the improved sulfur utilization for NCNT@Co-SnS₂ electrode is mainly resulted from the catalytic effect of NCNT/Co-SnS₂ on facilitating the electrochemical kinetics of the interconversion from polysulfides to Li₂S. Additionally, the sulfur feature at 2471.6 eV re-appeared and the features at 2472.9 and 2475.4 eV disappeared in the S K-edge XANES of S/CP@NCNT@Co-SnS₂ at the end of the charging process, demonstrating that Li₂S can be oxidized back to elemental sulfur during the following charge process, which is critical in maintaining the high capacity output during cycling.

The excellent electrochemical performance of the Li-S batteries assembled with S/NCNT@Co-SnS₂ can be attributed to the synergistic effects between (i) effective confinement of the soluble polysulfides in the cathode and (ii) the catalytic conversion from polysulfides to Li₂S, as schematically illustrated in **Figure 4**. The polar Co-SnS₂ in the S/NCNT@Co-SnS₂ electrode exhibits strong chemical interaction with the soluble polysulfides, which prevents polysulfide diffusion outside of

cathode. Consequently, loss of active materials during cycling is reduced; Li metal corrosion by polysulfide is minimized; and cycling stability is ultimately enhanced. Moreover, benefiting from the catalytic effect of Co-SnS₂ on the electrochemical conversion from polysulfides to Li₂S, more active materials are able to undergo complete redox reactions to increase sulfur utilization. The insoluble discharge productions, namely, Li₂S₂ and Li₂S, selectively deposit along the NCNTs and maintain the clear Li⁺ transport channels, so that C-rate performance is enhanced. This work is expected to open a new option for designing Li-S batteries with high active materials utilization and long-term cycling performance, and may shed light on the research and development of other energy storage devices.

3. Conclusion

In summary, the S/NCNT@Co-SnS₂ material acted as not only an effective shuttle-suppressing shield for polysulfide but also an electrocatalyst in improving sulfur utilization and cycling stability for high-sulfur-loading Li-S batteries. The results have demonstrated that the Co-doping can improve the chemical interaction between the SnS₂ and polysulfides, thereby confining polysulfide in the cathode and suppressing the shuttling effects. Furthermore, the cobalt-doped SnS₂ can serve as an effective catalyst by facilitating the conversion reaction between polysulfides and Li₂S, thereby promoting higher sulfur utilization and higher specific capacity. The Li-S batteries of S/NCNT@Co-SnS₂ electrode with 3 mg cm⁻² sulfur loading deliver a high initial discharge capacity of 1337.1 mA h g⁻¹ (excluding the capacity contribution from Co-SnS₂) and maintain 1004.3 mA h g⁻¹ after 100 cycles at a current density of 1.3 mA cm⁻². This is much higher than that of the Co-free S/NCNT@SnS₂ (initially 1074.7 mA h g⁻¹ and 843 mA h g⁻¹ at the 100th cycle) and S/NCNT (1000 mA h g⁻¹ initially and 663 mA h g⁻¹ at the 100th cycle) electrodes. Moreover, the S/NCNT@Co-SnS₂ cathode demonstrates a capacity decay of 0.16% per cycle over 300 cycles at 3.2 mA cm⁻². Even at a

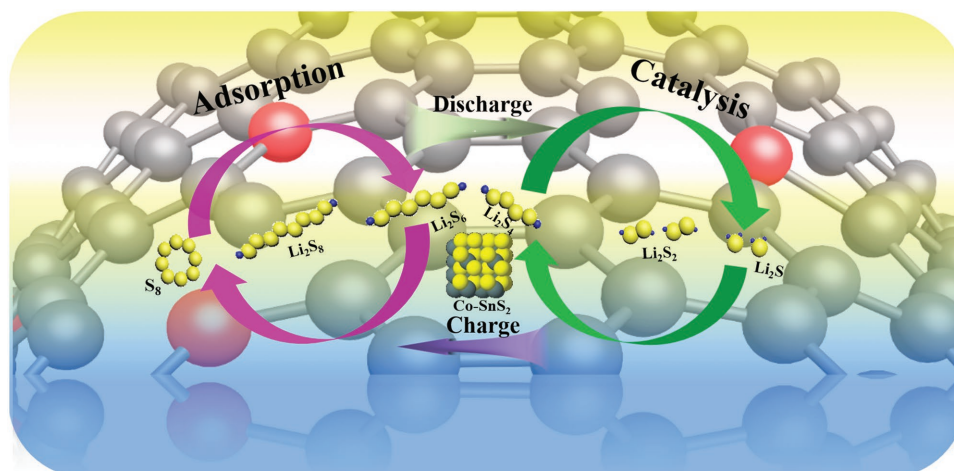


Figure 4. Schematic illustration of the charge/discharge process on S/NCNT@Co-SnS₂ electrode, including the chemical adsorption and catalytic conversion.

high current density of 5.1 mA cm⁻², a high discharge capacity of 722 mA h g⁻¹ is delivered. This work presents an effective strategy to improve the electrochemical performance of high-area-capacity Li-S batteries with high active materials utilization and excellent cycling stability.

4. Experimental Section

Synthesis of CP@NCNT: N-doped carbon nanotubes on carbon paper (named as CP@NCNT) were synthesized by an SPCVD method based on the previous reports.^[d] Briefly, atomic layer deposition (ALD) coatings were first conducted on CP in a Gemstar-8 ALD system (Arradance, USA). Al₂O₃ was deposited on the CP at 120 °C by using trimethylaluminum and water (H₂O) as precursors for 200 cycles. Then, the Al₂O₃ coated CP (2 × 8 cm²) was loaded into a vertical tube furnace that was ramped from room temperature to 856 °C under 200 mL min⁻¹ Ar flow. A catalytic ferrocene solution (solvent: acetonitrile, concentration: 0.02 g mL⁻¹) was subsequently introduced into the quartz tube at a flow rate of 0.1 mL min⁻¹ for 5 min under Ar atmosphere. Subsequently, imidazole solution was injected into the quartz tube (solvent: acetonitrile, concentration: 0.2 g mL⁻¹, flow rate: 0.1 mL min⁻¹) to grow CP@NCNT bundles for 30 min followed by cooling to room temperature. Typically, 30 min of growth yielded NCNT bundles with a length of ≈20–40 μm.

Synthesis of NCNT@SnS₂: Typically, 280 mg of SnCl₄·5 H₂O (0.8 × 10⁻³ M) and 210 mg thioacetamide (TAA) (2.8 × 10⁻³ M) were added into 50 mL ethanol and then magnetic stirred for 10 min. The mixture was submerged into an oil bath at 80 °C and vigorously stirred until the solution boiling. A piece of CP@NCNT was subsequently submerged into the boiling solution for 40 min under 80 °C. The resulting NCNT@SnS₂ was washed with deionized water and ethanol several times and dried in a vacuum oven at 60 °C for 24 h.

Synthesis of NCNT@SnS₂-H: The procedures were the same as the preparation of NCNT@SnS₂. The mass of SnCl₄·5 H₂O and TAA were changed to 560 mg (1.6 × 10⁻³ M) and 420 mg (5.6 × 10⁻³ M) respectively.

Synthesis of NCNT@Co-SnS₂: Typically, 216 mg of SnCl₄·5 H₂O (0.62 × 10⁻³ M), 42 mg of CoCl₂·6H₂O (0.18 × 10⁻³ M), and 210 mg of TAA (2.8 × 10⁻³ M) were added into 50 mL of ethanol for 40 min magnetic stirring. The subsequent procedures were similar to the preparation of NCNT@SnS₂.

Sulfur Impregnation: Firstly, the 100 mg sulfur was dissolve in 5 mL CS₂ solvent and obtained a uniform solution. Then, 120 μL above solution was absorbed by the as prepared electrodes (surface area: 0.785 cm²). After solvent removal, electrodes with a sulfur loading of 3 mg cm⁻² were obtained.

Characterizations: The morphologies of the samples were characterized by a Hitachi S-4800 field emission scanning electron microscope. Sulfur K-edge, tin L₃-edge, and Co K-edge spectra were conducted on the Soft X-ray Microcharacterization Beamline with different values of photo energy at the Canadian Light Source at the University of Saskatchewan in Saskatoon. Before synchrotron radiation experiments, original electrodes before and after battery test one cycles were prepared under protected environment in order to avoid oxidation of samples, the electrodes after discharge–charge processes were obtained from disassembled CR2032 coin cells and sealed in glovebox under Argon, and then transferred to the corresponding beamlines for further measurements.

Electrochemical Measurements: The electrochemical performance of the S/NCNT@Co-SnS₂, S/NCNT@SnS₂, S/NCNT@SnS₂-H, and S/NCNT cathodes was tested with CR2032 coin cells, fabricated in an Ar-filled glovebox. The cathode and Li anode were separated by a polypropylene membrane (Celgard 2400). The electrolyte used in this study was 1 M bis (trifluoromethylsulfonyl) imide in DME/1,3-dioxolane (1:1 v/v) with 1 wt% LiNO₃ additive, and the electrolyte/sulfur ratio was controlled as around 15.3 μL mg⁻¹ for S/NCNT@Co-SnS₂, S/NCNT@SnS₂, S/NCNT@SnS₂-H, and S/NCNT electrodes. EIS was tested at open-circuit with a frequency range of 5.0 × 10⁵ Hz to 1.0 × 10⁻² Hz on a versatile multichannel potentiostation 3/Z (VMP3). CV of S/NCNT@Co-SnS₂ and S/NCNT@SnS₂ was performed on the same instrument and the data were collected under a scanning rate of 0.1 mV s⁻¹ between 1.7 and 2.8 V. The charge–discharge tests were carried out using a LAND CT-2001A system with voltages between 1.7 and 2.8 V at room temperature. Unless otherwise specified, the specific capacities reported in this work were calculated based on sulfur and the voltages versus Li⁺/Li.

Supporting Information

Supporting Information is available from the Wiley Online Library or from the author.

Acknowledgements

X.G. and X.Y. contributed equally to this work. This research was supported by the Natural Science and Engineering Research Council of Canada (NSERC), the Canada Research Chair Program (CRC), and the Canada Foundation for Innovation (CFI); research conducted at the Canada Light Source was supported by CIHR, NRC, NSERC, and the University of Saskatchewan. X.G. acknowledges financial support from

the Chinese Scholarship Council to conduct research at the University of Western Ontario.

Conflict of Interest

The authors declare no conflict of interest.

Keywords

absorption effects, cobalt-doped SnS₂, electrocatalyst effects, high sulfur loading, Li sulfur batteries

Received: September 23, 2018

Revised: December 18, 2018

Published online:

- [1] a) X. Liu, J. Q. Huang, Q. Zhang, L. Mai, *Adv. Mater.* **2017**, *29*, 1601759; b) A. Manthiram, Y. Fu, S. H. Chung, C. Zu, Y. S. Su, *Chem. Rev.* **2014**, *114*, 11751; c) H. Lin, L. Yang, X. Jiang, G. Li, T. Zhang, Q. Yao, G. W. Zheng, J. Y. Lee, *Energy Environ. Sci.* **2017**, *10*, 1476; d) Y. Zhao, X. Yang, L. Y. Kuo, P. Kaghazchi, Q. Sun, J. Liang, B. Wang, A. Lushington, R. Li, H. Zhang, X. Sun, *Small* **2018**, *14*, 1703717; e) L. Li, L. Chen, S. Mukherjee, J. Gao, H. Sun, Z. Liu, X. Ma, T. Gupta, C. V. Singh, W. Ren, H. M. Cheng, N. Koratkar, *Adv. Mater.* **2017**, *29*, 1602734; f) X. Yang, Y. Yu, X. Lin, J. Liang, K. Adair, Y. Zhao, C. Wang, X. Li, Q. Sun, H. Zhang, X. Li, R. Li, H. Zhang, X. Sun, *J. Mater. Chem. A* **2018**, *6*, 22958; g) S. Wang, F. Gong, S. Yang, J. Liao, M. Wu, Z. Xu, C. Chen, X. Yang, F. Zhao, B. Wang, Y. Wang, X. Sun, *Adv. Funct. Mater.* **2018**, *28*, 1801806.
- [2] R. Fang, S. Zhao, P. Hou, M. Cheng, S. Wang, H. M. Cheng, C. Liu, F. Li, *Adv. Mater.* **2016**, *28*, 3374.
- [3] a) S. Zhang, Z. P. Yao, *Anal. Chim. Acta* **2012**, *711*, 77; b) H. Wang, Y. Yang, Y. Liang, J. T. Robinson, Y. Li, A. Jackson, Y. Cui, H. Dai, *Nano Lett.* **2011**, *11*, 2644.
- [4] D. Liu, C. Zhang, G. Zhou, W. Lv, G. Ling, L. Zhi, Q. H. Yang, *Adv. Sci.* **2018**, *5*, 1700270.
- [5] a) X. Ji, K. T. Lee, L. F. Nazar, *Nat. Mater.* **2009**, *8*, 500; b) X. Yang, N. Yan, W. Zhou, H. Zhang, X. Li, H. Zhang, *J. Mater. Chem. A* **2015**, *3*, 15314; c) X. Yang, B. Dong, H. Zhang, R. Ge, Y. Gao, H. Zhang, *RSC Adv.* **2015**, *5*, 86137; d) Q. Pang, X. Liang, C. Y. Kwok, L. F. Nazar, *Nat. Energy* **2016**, *1*, 16132; e) X. Yang, X. Li, K. Adair, H. Zhang, X. Sun, *Electrochem. Energy Rev.* **2018**, *1*, 239; f) A. Eftekhari, Z. Fan, *Mater. Chem. Front.* **2017**, *1*, 1001.
- [6] a) Z. Li, J. Zhang, X. W. Lou, *Angew. Chem., Int. Ed.* **2015**, *54*, 12886; b) Z. Wei Seh, W. Li, J. J. Cha, G. Zheng, Y. Yang, M. T. McDowell, P. C. Hsu, Y. Cui, *Nat. Commun.* **2013**, *4*, 1331; c) M. Xiang, H. Wu, H. Liu, J. Huang, Y. Zheng, L. Yang, P. Jing, Y. Zhang, S. Dou, H. Liu, *Adv. Funct. Mater.* **2017**, *27*, 1702573.
- [7] a) J. Zhang, C. You, W. Zhang, J. Wang, S. Guo, R. Yang, Y. Xu, *Electrochim. Acta* **2017**, *250*, 159; b) L. Ma, H. Yuan, W. Zhang, G. Zhu, Y. Wang, Y. Hu, P. Zhao, R. Chen, T. Chen, J. Liu, Z. Hu, Z. Jin, *Nano Lett.* **2017**, *17*, 7839.
- [8] a) M. Li, J. Zhou, J. Zhou, C. Guo, Y. Han, Y. Zhu, G. Wang, Y. Qian, *Mater. Res. Bull.* **2017**, *96*, 509; b) X. Li, Y. Lu, Z. Hou, W. Zhang, Y. Zhu, Y. Qian, J. Liang, Y. Qian, *ACS Appl. Mater. Interfaces* **2016**, *8*, 19550; c) X. Li, L. Chu, Y. Wang, L. Pan, *Mater. Sci. Eng., B* **2016**, *205*, 46; d) Q. Wang, R. Zou, W. Xia, J. Ma, B. Qiu, A. Mahmood, R. Zhao, Y. Yang, D. Xia, Q. Xu, *Small* **2015**, *11*, 2511.
- [9] J. Zhou, X. Liu, L. Zhu, J. Zhou, Y. Guan, L. Chen, S. Niu, J. Cai, D. Sun, Y. Zhu, J. Du, G. Wang, Y. Qian, *Joule* **2018**, *2*, 2681.
- [10] a) Y. Zhong, L. Yin, P. He, W. Liu, Z. Wu, H. Wang, *J. Am. Chem. Soc.* **2018**, *140*, 1455; b) Z. Yuan, H. J. Peng, T. Z. Hou, J. Q. Huang, C. M. Chen, D. W. Wang, X. B. Cheng, F. Wei, Q. Zhang, *Nano Lett.* **2016**, *16*, 519.
- [11] a) X. Yang, Y. Chen, M. Wang, H. Zhang, X. Li, H. Zhang, *Adv. Funct. Mater.* **2016**, *26*, 8427; b) X. Yang, Y. Yu, N. Yan, H. Zhang, X. Li, H. Zhang, *J. Mater. Chem. A* **2016**, *4*, 5965; c) X. Yang, H. Zhang, Y. Chen, Y. Yu, X. Li, H. Zhang, *Nano Energy* **2017**, *39*, 418.
- [12] Y. Li, K. K. Fu, C. Chen, W. Luo, T. Gao, S. Xu, J. Dai, G. Pastel, Y. Wang, B. Liu, J. Song, Y. Chen, C. Yang, L. Hu, *ACS Nano* **2017**, *11*, 4801.
- [13] A. Eftekhari, *Sustainable Energy Fuels* **2017**, *1*, 2053.
- [14] a) L. Luo, S.-H. Chung, A. Manthiram, *Adv. Energy Mater.* **2018**, *8*, 1801014; b) Q. Zhang, Y. Wang, Z. W. Seh, Z. Fu, R. Zhang, Y. Cui, *Nano Lett.* **2015**, *15*, 3780.
- [15] A. Eftekhari, D.-W. Kim, *J. Mater. Chem. A* **2017**, *5*, 17734.
- [16] a) Y. Yan, M. Shi, Y. Wei, C. Zhao, M. Carnie, R. Yang, Y. Xu, *J. Alloys Compd.* **2018**, *738*, 16; b) D. R. Deng, T.-H. An, Y.-J. Li, Q.-H. Wu, M.-S. Zheng, Q. F. Dong, *J. Mater. Chem. A* **2016**, *4*, 16184.
- [17] a) Z. Lin, C. Nan, Y. Ye, J. Guo, J. Zhu, E. J. Cairns, *Nano Energy* **2014**, *9*, 408; b) X. Feng, M. K. Song, W. C. Stolte, D. Gardenghi, D. Zhang, X. Sun, J. Zhu, E. J. Cairns, J. Guo, *Phys. Chem. Chem. Phys.* **2014**, *16*, 16931.
- [18] a) M. Cuisinier, P.-E. Cabelguen, S. Evers, G. He, M. Kolbeck, A. Garsuch, T. Bolin, M. Balasubramanian, L. F. Nazar, *J. Phys. Chem. Lett.* **2013**, *4*, 3227; b) M. U. Patel, I. Arcon, G. Aquilanti, L. Stievano, G. Mali, R. Dominko, *ChemPhysChem* **2014**, *15*, 894.
- [19] X. Li, A. Lushington, Q. Sun, W. Xiao, J. Liu, B. Wang, Y. Ye, K. Nie, Y. Hu, Q. Xiao, R. Li, J. Guo, T. K. Sham, X. Sun, *Nano Lett.* **2016**, *16*, 3545.
- [20] M. Vijayakumar, N. Govind, E. Walter, S. D. Burton, A. Shukla, A. Devaraj, J. Xiao, J. Liu, C. Wang, A. Karim, S. Thevuthasan, *Phys. Chem. Chem. Phys.* **2014**, *16*, 10923.